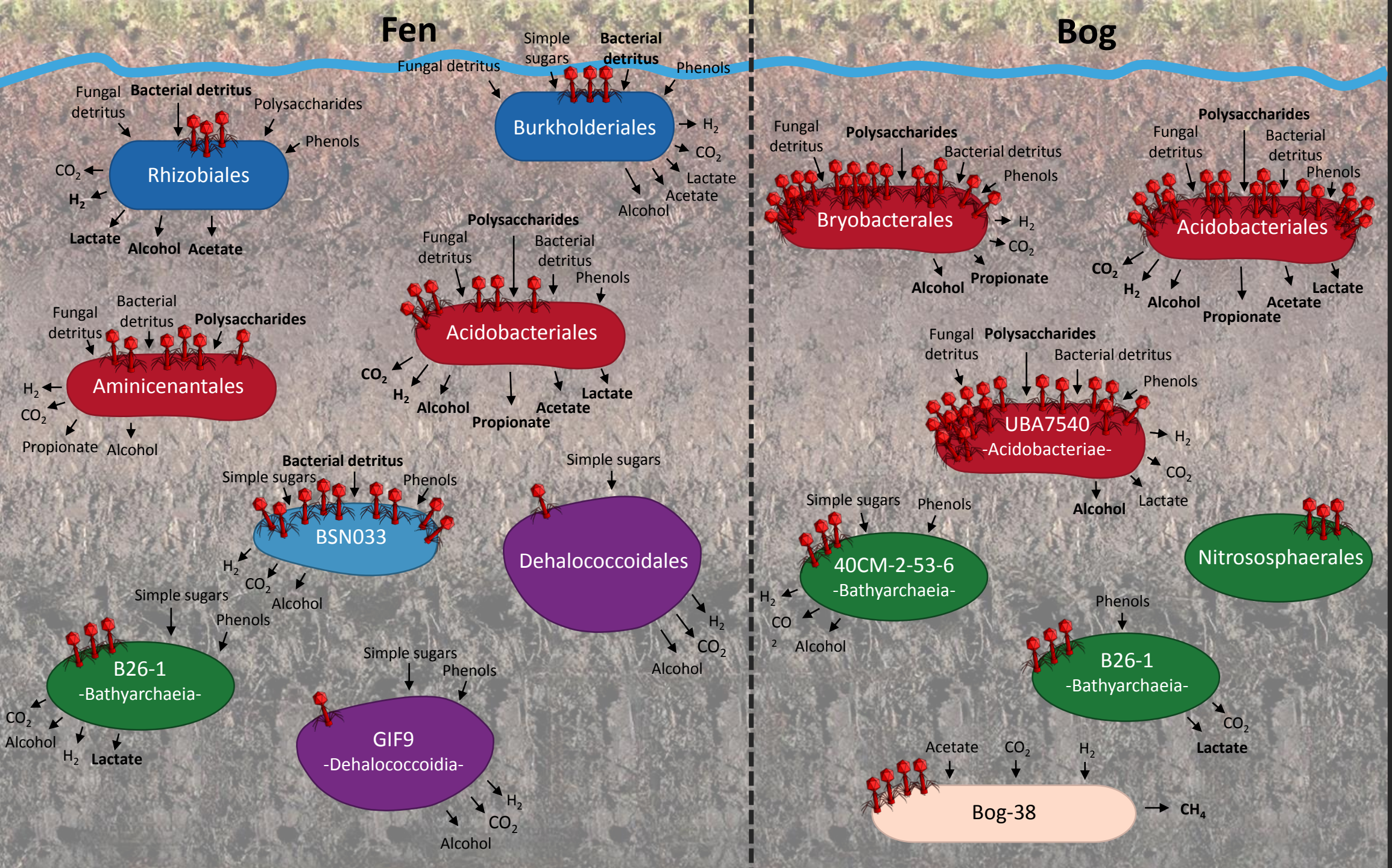
Fen
Bog
Water-table depth
fen/bog delimitation
Virus
Proteobacteria
Acidobacteriota
Desulfobacterota
Chloroflexota
Crenarchaeota
Halobacterota
Rhizobiales
Fungal detritus
Bacterial detritus
Polysaccharides
Phenols
Lactate
Alcohol
Acetate
Burkholderiales
Simple sugars
Aminicenantales
Propionate
Acidobacteriales
Propionate
BSN033
Dehalococcoidales
B26-1
-Bathyarchaeia-
GIF9
-Dehalococcoidia-
Bryobacterales
Propionate
UBA7540
-Acidobacteriae-
40CM-2-53-6
-Bathyarchaeia-
Nitrososphaerales
Bog-38

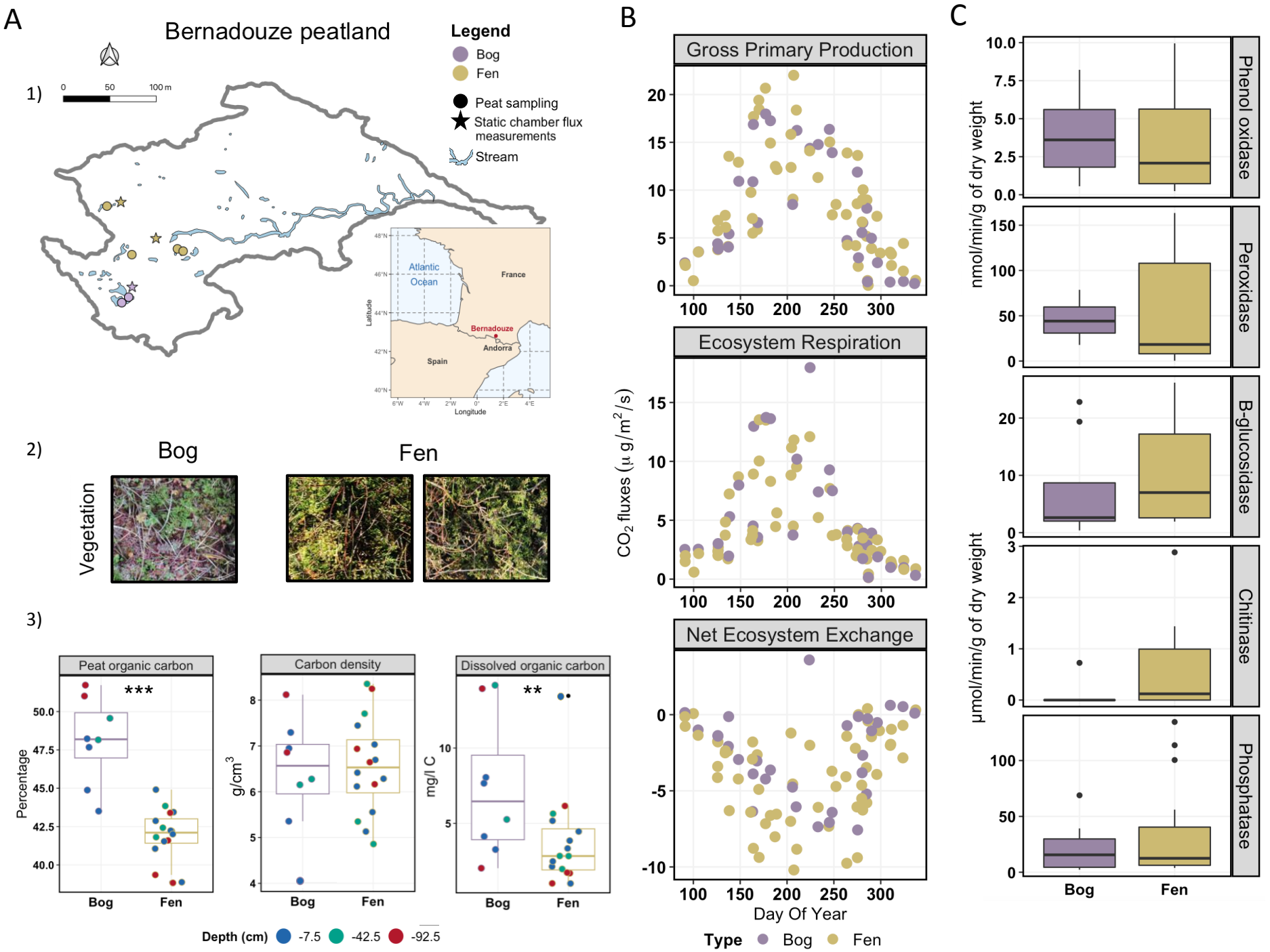

Figure 1. Location of the Bernadouze peatland and carbon dynamics (peat organic carbon, dissolved organic carbon, atmospheric carbon fluxes and microbial enzymatic activities related to OM degradation).

*A. 1) Location of the Bernadouze peatland and sampling sites. The dots represent the locations of peat samplings and the stars the location of static chamber flux measurements. Purple and yellow color code indicates the bog and fen sites respectively. 2) Representative vegetation covers of the bog and the fen. 3) Box plots of peat organic carbon and dissolved organic carbon concentration, with n=8 for bog and n=16 for fen. Stars indicate the level of significance (** if p-value < 0.01 and *** if p-value < 0.001).*

B. Atmospheric carbon fluxes over six-year period. Gross Primary Production (GPP), Ecosystem Respiration (ER) and Net Ecosystem Exchange (NEE), measured in the bog (30 measures across 6 years) and the fen (57 measures across 6 years) using a static chamber flux.

C. Comparison of enzymatic activities involved in the degradation of organic matter between bog (n=8) and fen (n=16).

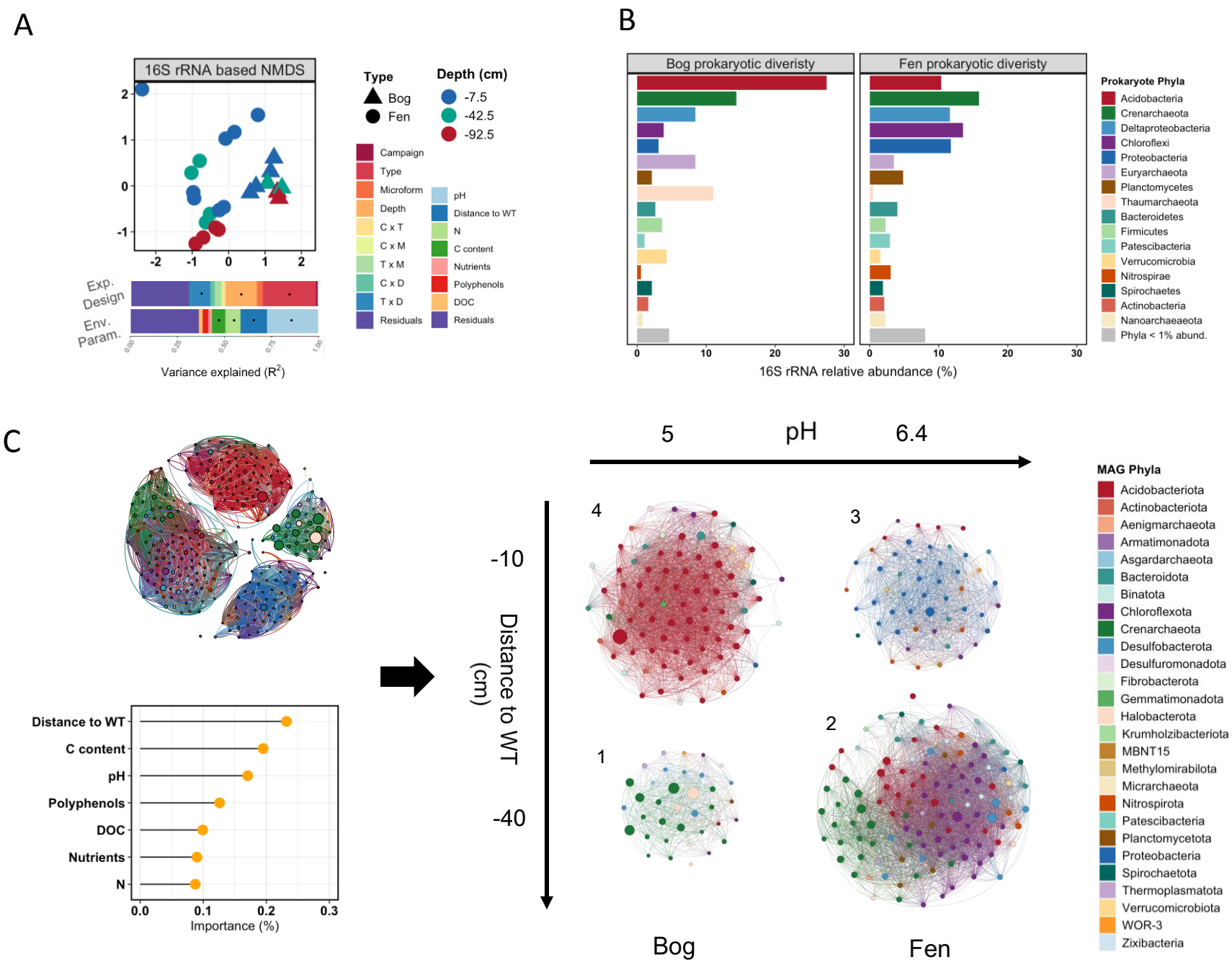

Figure 2. Environmental drivers of the microbial communities, prokaryotic diversity based on 16S rRNA gene and characterization of the Bernadouze metagenome-assembled genomes (290 dereplicated MAGs).

A. Non-metric multidimensional scaling (NMDS) plot of 16S rRNA gene data based on Bray-Curtis distance (stress: 0.10). Below the NMDS, analyses of variance testing the effect of experimental design (Exp. Design): campaign, peatland type, microform, depth, and all possible two-way interactions, and environmental variables (Env. Param.): pH, distance to WT, DOC, C content, N, polyphenols, nutrients, on microbial community structure (16S rRNA based data) using PerMANOVA. Black dots indicate significant correlations (if p-value < 0.05).

B. Relative abundance of prokaryotic phyla in the bog and the fen, estimated by unassembled 16S rRNA gene reads.

C. Abundance-weighted co-occurrence network based on Spearman correlations calculated from the recruitment values of the 290 unique MAGs with > 50% of completeness and < 5% of contamination (top left). Only significant edges are shown (coefficient > 0.6, p-value < 0.001). The size of the nodes is proportional to the cumulative abundance of MAGs in the 24 metagenomes. The importance of environmental variables predicting module configuration, estimated by a random forest classification model, is shown in the bottom left. Spatial location of MAGs was estimated using individual weighted means calculated for each environmental variable (pH and distance to WT) using RPKG data as abundance (right).

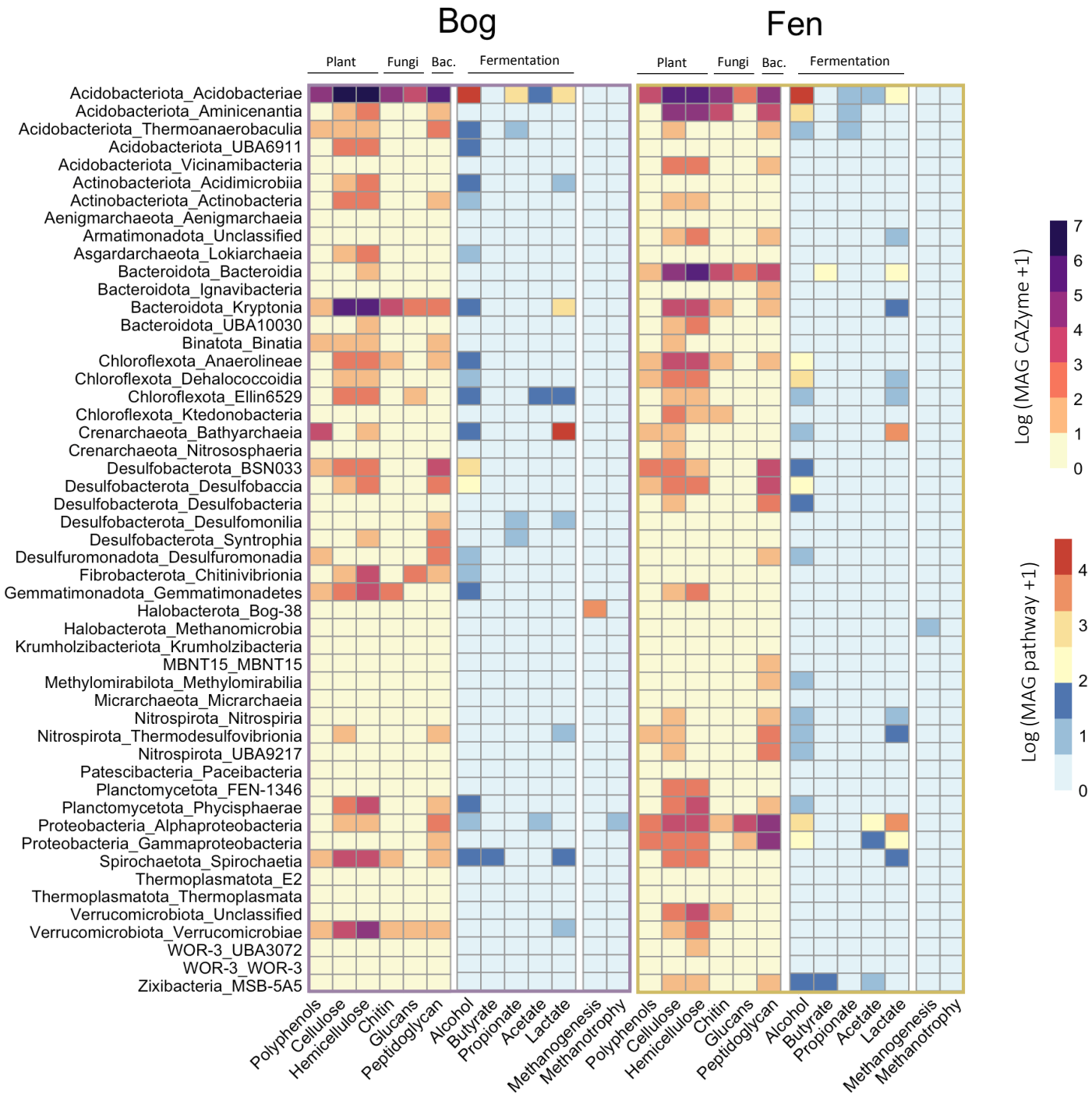

Figure 3. Predicted metabolic capacities of the Bernadouze MAGs.
Heatmap showing the abundance (log (abundance +1)) of MAGs-encoded CAZyme involved in plant biomass degradation (cellulose: GH1, GH3, GH116, GH5, GH6, GH9, GH12, GH45, GH8, AA9, AA10, GH7, GH48, hemicellulose: GH36, GH51, GH54, GH62, GH95, CE1, CE2, CE3, CE4, CE5, CE6, CE7, CE12, CE15, CE16, GH2, GH52, GH120, GH39, GH43, GH26, GH10, GH11, GH30, GH131, GH67, GH115, GH74, GH16, GH44, AA6), fungal biomass degradation (chitin: GH18, GH19, AA11, GH20 and glucans: GH17, GH64, GH81, GH128, GH55), bacterial biomass degradation (peptidoglycan: GH22, GH24, GH25, GH108, GH23, GH73, GH102, GH103, GH104) and polyphenol compounds degradation (K05909, AA1, AA2, K00422) in yellow to purple. The abundances of fermentative (alcohol: K00001, K00121, K04072, K13951, K13952, K13953, K13954, K13980, K18857, butyrate: K00634, K00929, K01896, propionate: K19697, K01026, acetate: K00625, K00925, K01905, K01067, lactate: K00016, K00101, K03778, K03777), methanogenic (K00399, K00401, K00402) and methanotrophic (K10944, K10945, K10946) pathways recovered in MAGs are in light blue to red. The metabolic capacities of MAGs in bog are shown in the left panels (purple frame) and in the right panels (yellow frame) for the fen. These capacities are summed at class-level and log transformed +1.

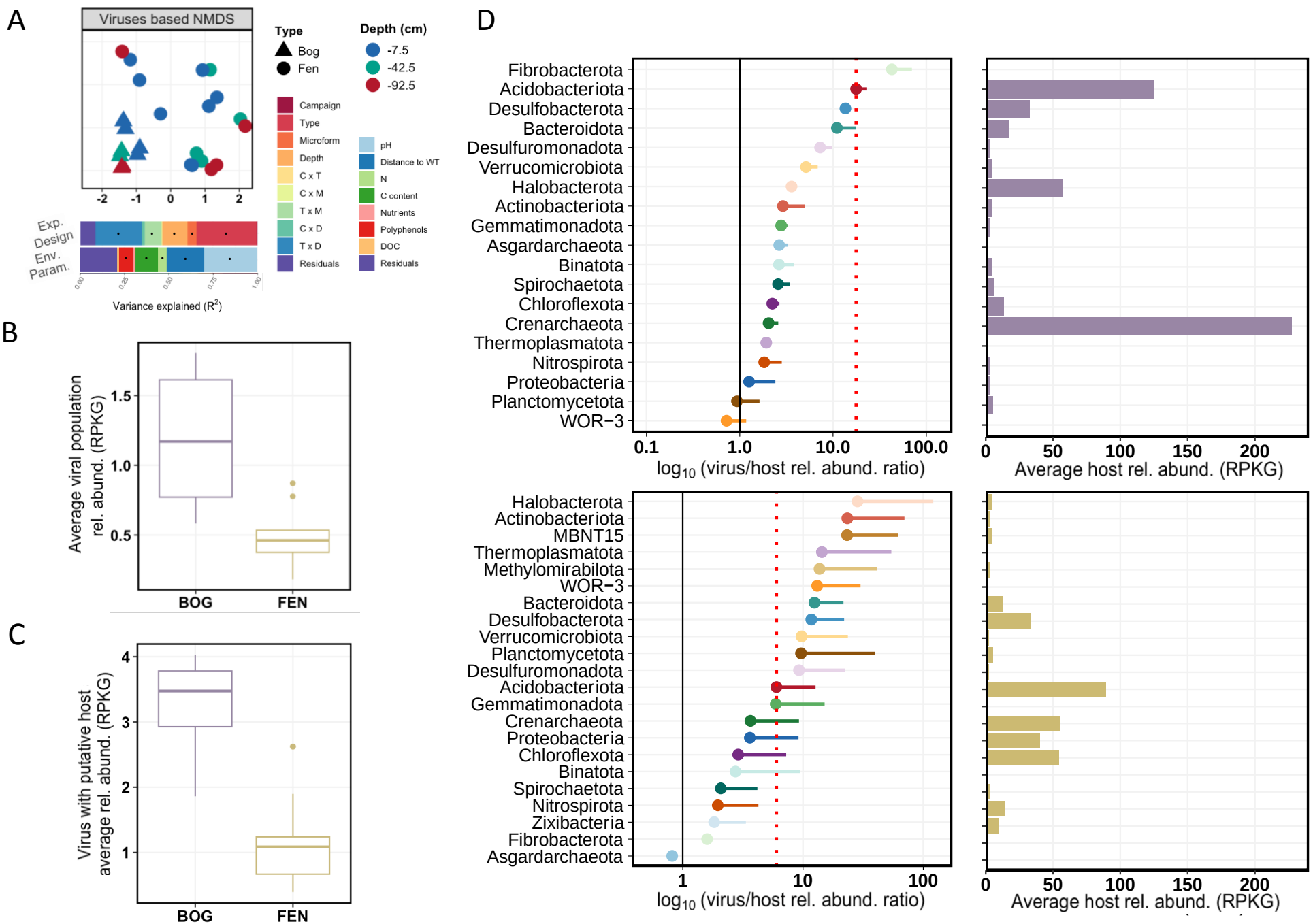

Figure 4. Environmental drivers and distribution of the viral populations at Bernadouze, predicted prokaryotic host and host-virus relationships in bog and fen

NMDS plot of the viral populations using Bray-Curtis distance (stress: 0.08). Below the NMDS, analyses of variance testing the effect of experimental design (Exp. Design): campaign, peatland type, microform, depth and all possible two-way interactions, and environmental variables (Env. Param.): pH, distance to WT, DOC, C content, N, polyphenols, nutrients, on viral composition using PerMANOVA. Black dots indicate significant correlation (if p-value < 0.05). Average viral population abundance in bog and fen samples (expressed in RPKG). Box plot representing the average abundance of the virus for which a putative host was identified (expressed in RPKG). Virus/host abundance ratios by host lineage. Abundances were calculated from read mapping to viral population and host genomes (both expressed in RPKG), respectively, in bog (top left panel) and in fen (bottom left panel). The dots indicate the mean ratio across samples (in bog n = 8, in fen n = 16), and the error bars indicate one standard deviation. The red line indicates the virus/host abundance ratio for the Acidobacteria phylum. The means host abundance in bog and fen are reported on the right panels.

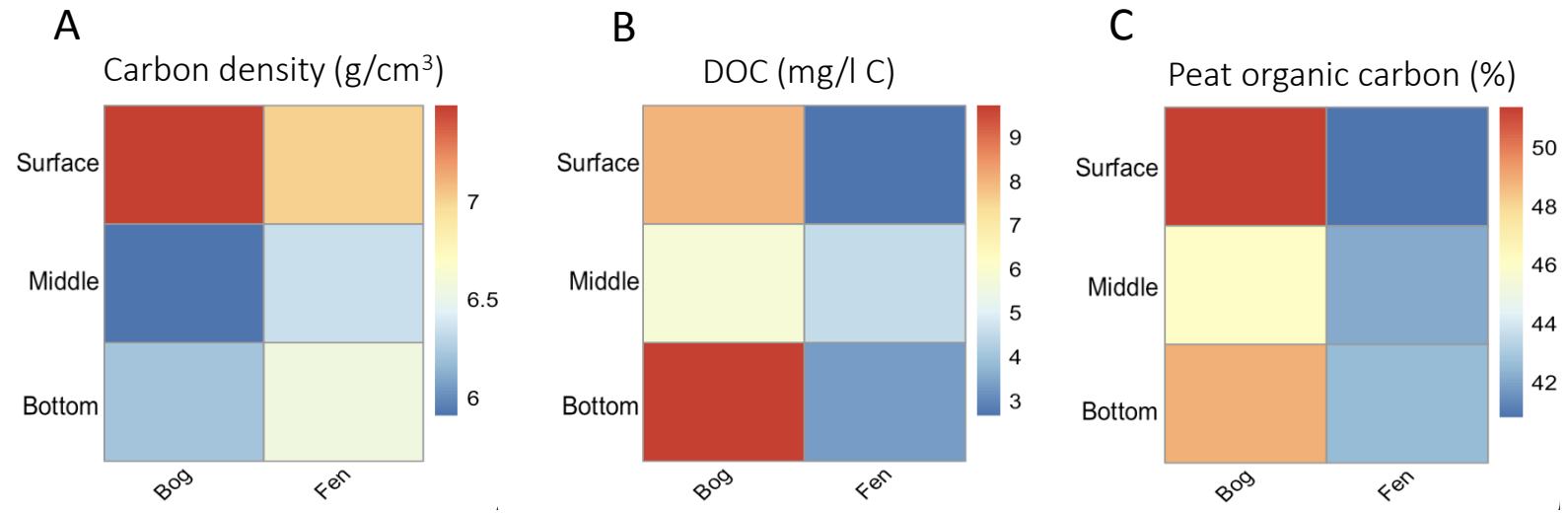

Figure S1. Carbon variations in bog and fens according to peat depth

Heatmap showing the variations of carbon density (A), dissolved organic carbon (B) and peat organic carbon (C) in bog (n=8) and fen (n=16).

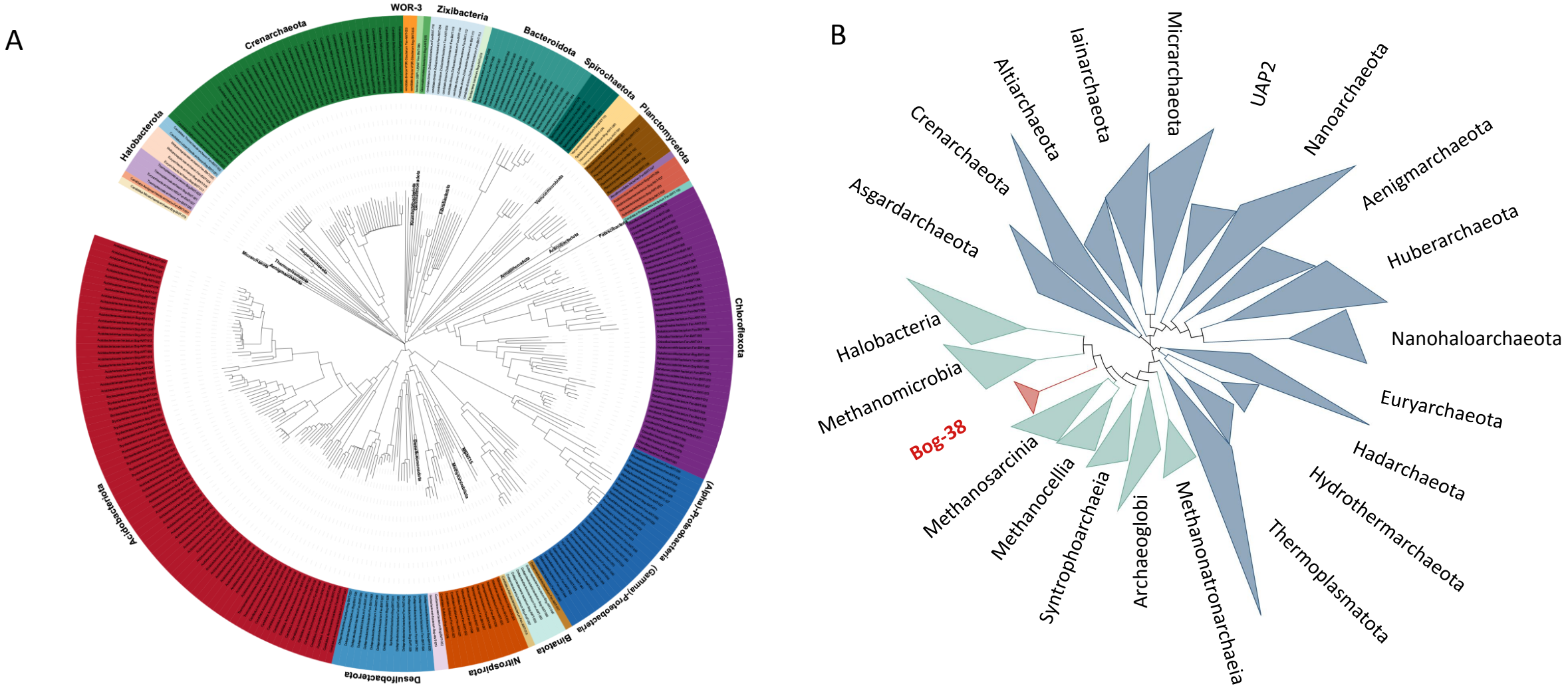

Figure S2. Maximum likelihood phylogenomic tree of the MAGs recovered from the Bernadouze peatland and position of the Bernadouze methanogen lineages within the archaeal phylogenetic tree

Maximum likelihood phylogenomic tree computed using GTDB-tk software, classifying each MAG according to its location in the reference tree, its relative evolutionary divergence and/or average nucleotide identity (ANI) with respect to the reference genomes. The tree was estimated based on the concatenated phylogeny of 120 bacterial single-copy marker genes or 122 archaeal single-copy marker genes. It includes 240 unique bacterial genomes and 50 unique archaeal genomes (> 50% of completeness and < 5% of contamination). Among them, Acidobacteriota (80 MAGs), Chloroflexota (44), Crenarchaeota (38), Proteobacteria (29), Bacteroidota (16) and Desulfobacterota (14) are the most represented phyla in the assemblage. In addition, 25 genomes belonging to phyla with a relative abundance of less than 1% according to 16S rRNA gene data were assembled, among which Aenigmarchaeota and Micrarchaeota (DPANN), Asgardarchaeota, Armatimonadota, Gemmatimonadota or Krumholzibacteriota.

Phylogenetic tree of archaea calculated using GTDB-tk software. Reference taxa were also plotted to identify the position of Bernadouze's methanogen lineages. To highlight the position of Bog-38 (in red), the branches are collapsed either at the phylum-level (in blue) or the class-level (in green). Four MAGs exhibiting capacity for hydrogenotrophic methanogenesis were recovered, two belonging to the Bog-38 class and two to Methanomicrobia. The present tree revealed that Bog-38 is a sister taxon of the clade Methanomicrobia/Halobacteria. All these taxa share a common ancestor with the clade Methanosarcina/Methanocellia.

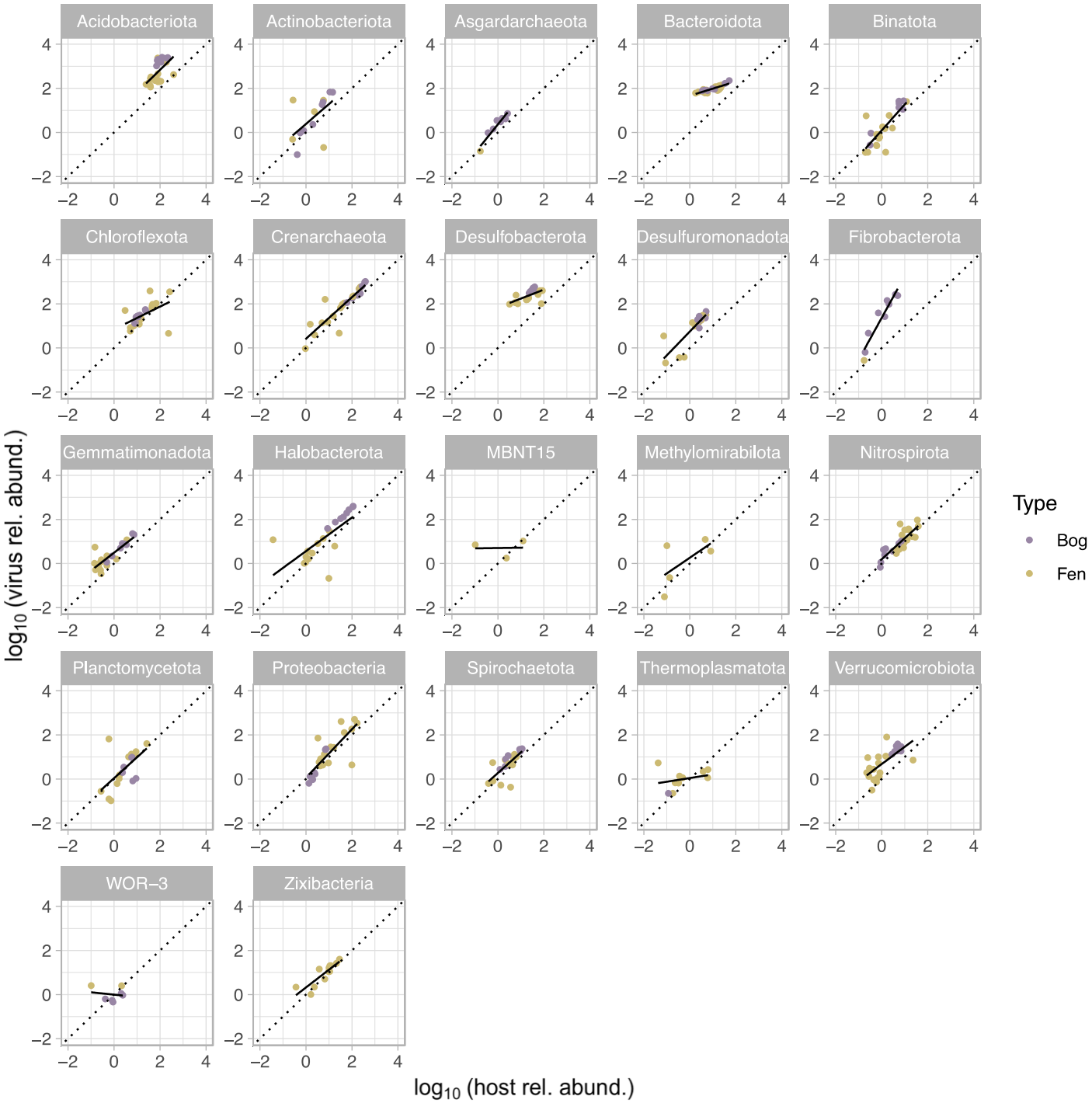

Figure S3. Host virus relationships in bog and fen

Positive relationships between virus abundance and host abundance at phylum level in the bog (n=8) and in the fen (n=16). Virus and host abundance were log-10 transformed. The dotted black line represents the 1:1 ratio, and the solid black line is the result of the linear regression. The bog samples are plotted in purple and the fen samples in yellow.

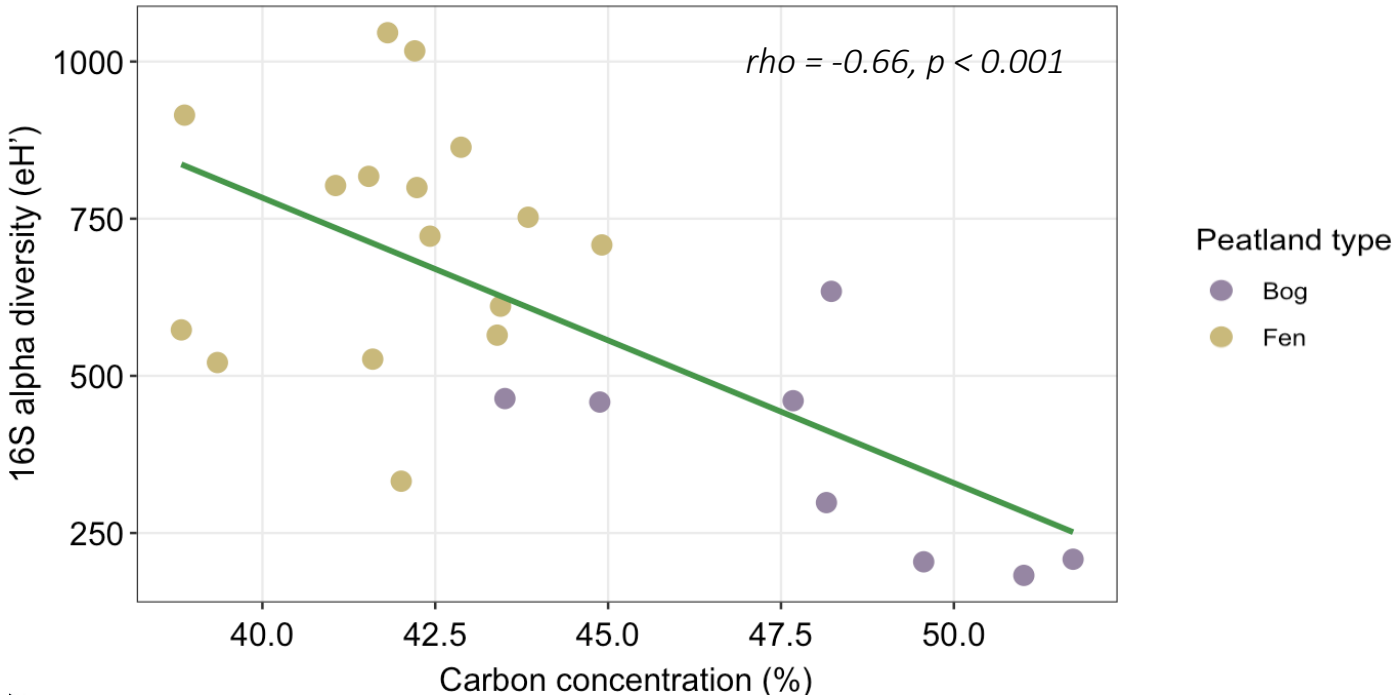

Figure S2. Relationship between carbon concentration and microbial diversity

Scatterplots of pairwise correlations illustrating the relationship between prokaryotic alpha diversity estimated from 16S rRNA (exponential of Shannon, eH') and carbon concentration. The slope of the linear regression is shown in green, and the associated statistical values from a Spearman's rank correlation test are displayed on the right.

A

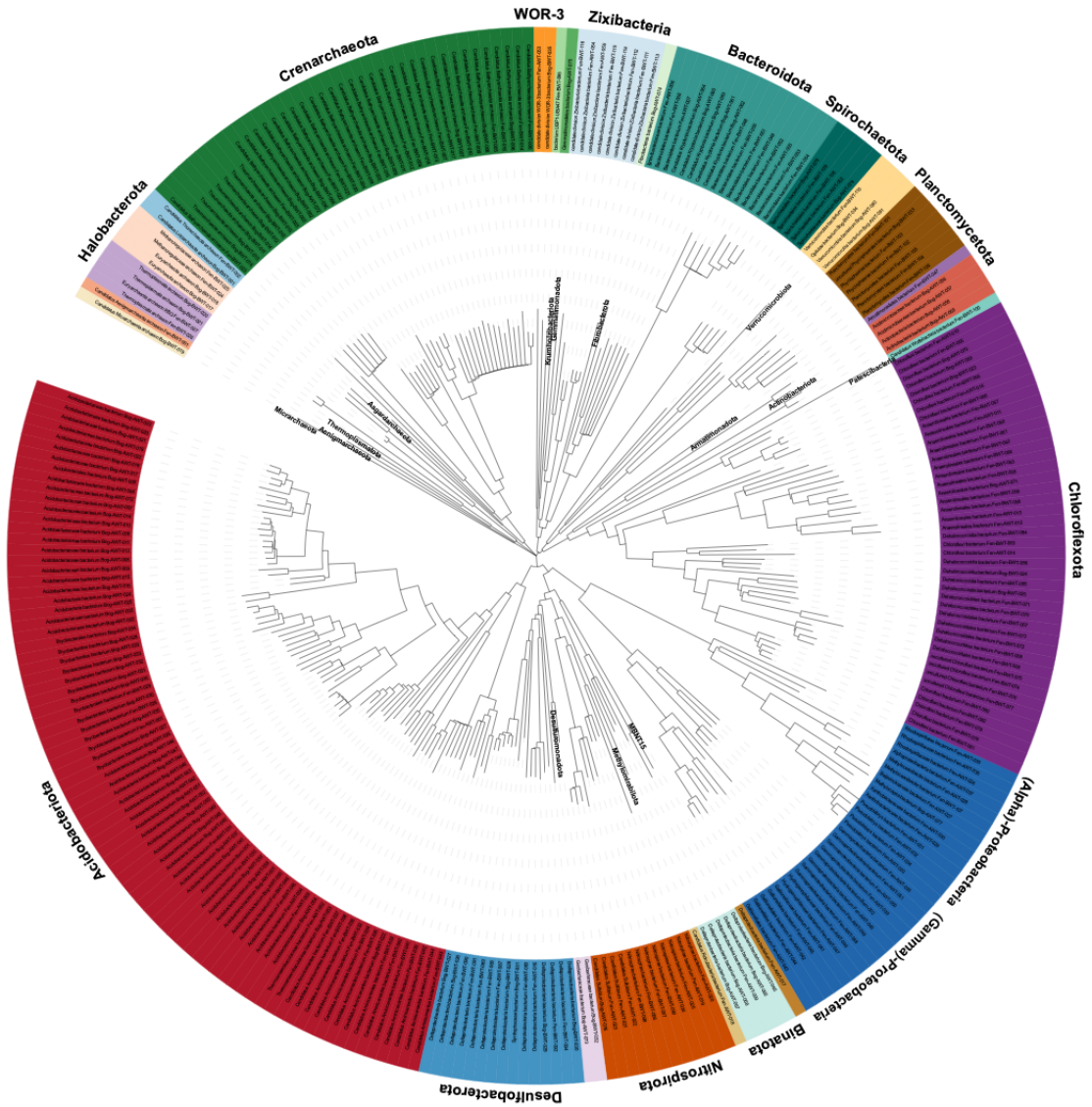
WOR-3
Zixibacteria
Bacteroidota
Spirochaetota
Planctomycetota
Chloroflexota
(Alpha)-Proteobacteria
(Gamma)-Proteobacteria
Bilatota
Nitrospirota
Desulfobacterota
Actinobacteriota
Halobacterota
Crenarchaeota

B

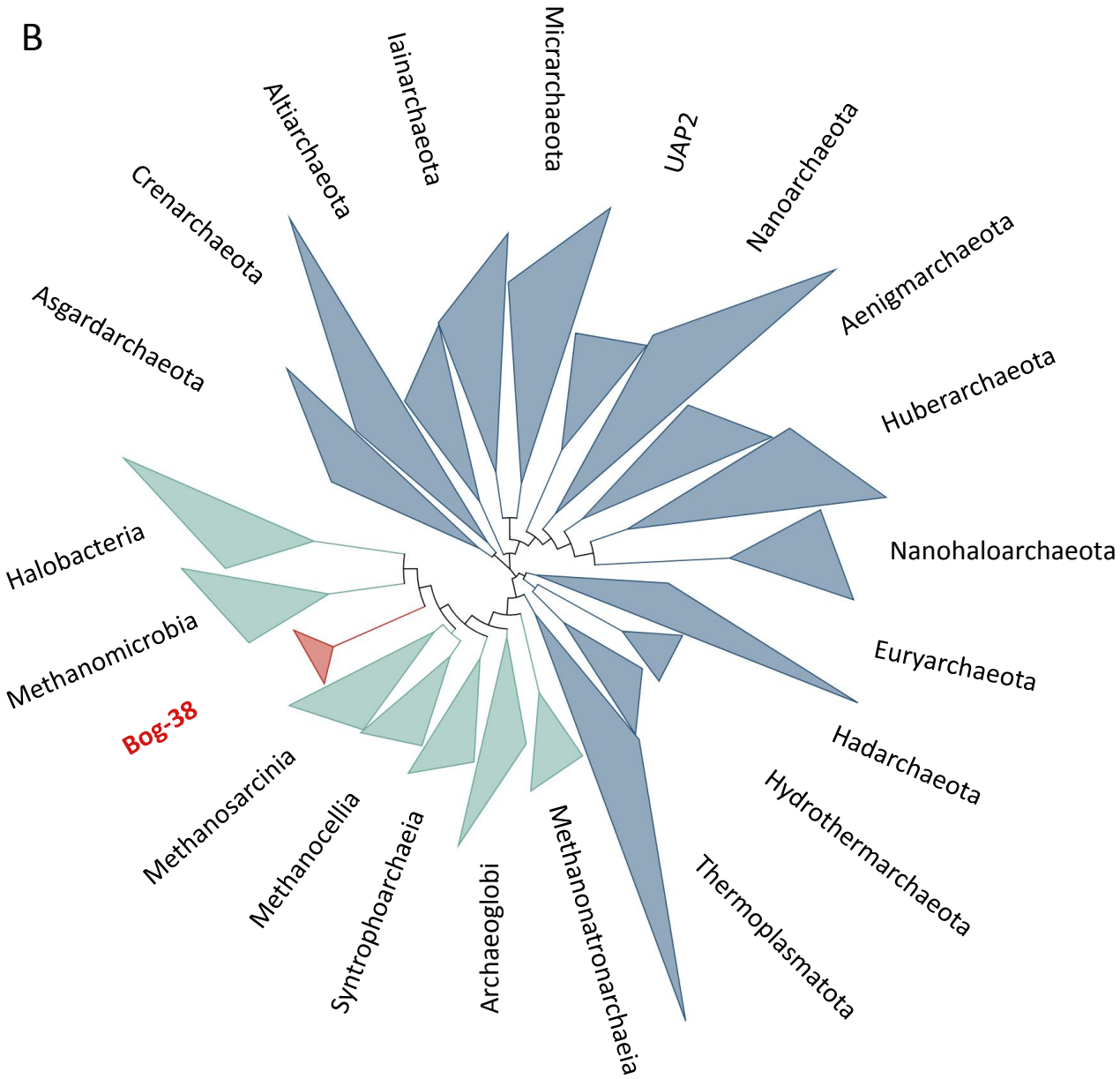
Micrarchaeota
Iainarchaeota
Altiarchaeota
Crenarchaeota
Asgardarchaeota
UAP2
Nanoarchaeota
Aenigmarchaeota
Huberarchaeota
Nanohaloarchaeota
Euryarchaeota
Hadarchaeota
Hydrothermarchaeota
Thermoplasmatota
Methanonatronarchaeia
Archaeoglobi
Syntrophoarchaeia
Methanocellia
Methanosarcinia
Bog-38
Methanomicrobia
Halobacteria